Manuscript Click here to view linked References

Optimizing multi-circuit transmission lines for single-phase auto-reclosing

Jhair S. Acosta, Maria C. Tavares, and Aniruddha M. Gole

***Abstract*—In this paper, novel multi-circuit transmission line (MCTL) designs with low secondary arc current (SAC) values are proposed. The Non-dominated Sorting Genetic Algorithm II (NSGA-II) was used to generate the optimized tower structures. The aim is to select the MCTL configuration that satisfies multiple objectives such as increased capacity, reduced cost, right-of-way (ROW), and tower height, while satisfying several constraints such as SAC limit, ampacity, electric field, etc. The objective function is formulated as a mathematical function of design variables such as sub-conductor position, phase arrangement, etc., and several constraints. Two-port theory is used to calculate the SAC resulting from different faults along the line, which is significantly faster compared with time-domain Electromagnetic Transient (EMT) simulations. Comparisons of MCTLs with and without SAC constraints are presented, clearly showing the importance of taking into account SAC limits during the optimization process. As a result, MCTL structures with SAC reductions of up-to 64% were obtained, indicating that the MCTL are able to successfully handle Single Phase Auto-Reclosing (SPAR).**

***Keywords*—Electromagnetic Transients Simulation, Optimization, Secondary arc, Single-phase auto-reclosing, Two-port networks.**

I. Introduction

THE first attempts for transmitting more power by means of modifying the bundle geometry of transmission lines were performed by Russian [1] and Brazilian [2]–[4] researchers, using High Surge Impedance Loading (HSIL) lines. Later researchers demonstrated that the HSIL lines do not aggravate the overvoltage response [5] resulting from switching events. In [6] the cost was optimized yielding an improved cost/MW ratio. Then, aiming to further reduce the right-of-way (ROW), optimized Multi-circuit Transmission lines (MCTLs) were proposed [7]–[10] as an improvement over single-circuit HSIL. Selecting the configuration of the multi-circuit line becomes more of a challenge when the individual circuits have different voltage levels. Such lines are referred to as multi-circuit multi voltage transmission lines (MCMVTL).

However, because of the capacitive and inductive intra-circuit and inter-circuit coupling in multi-circuit lines, the secondary arc current (SAC) is high, and creates a problem for single-phase auto-reclosing (SPAR). In some cases very high-value neutral reactor are specified, and even though it is not possible to reduce the SAC to adequate values. To solve the problem, this paper proposes to include the SAC limit as a restriction in the mathematical model presented in [9], mitigating SAC from its origin, at the tower design.

The main contributions of this paper are as follows:

1) Novel optimized MCTLs ready to perform SPAR.
2) Optimized MCTLs with SACs respecting the limits using conventional four-legged reactor schemes.

II. Single-phase auto reclosing (SPAR)

During a single line to ground (SLG) fault it is possible to maintain part of the power flow if only the faulty phase is opened. In single circuits 54% can be maintained, while in double circuits the value rises to 75% [11].

After a certain dead-time of the single phase tripping an auto reclosing attempt is performed. If the fault is eliminated, the system is back to normal operation. Otherwise, the sound phases must trip (three-phase tripping), to completely interrupt the power supply [12].

In the fault process, the current that appears before the breaker opening is referred to as the "primary arc current", and has a magnitude of several kA. After the opening of the faulty breaker poles at both line terminals there exist inductive and capacitive coupling between the faulty and sound phases (from the same circuit and from the other circuits). The coupling maintains a residual "secondary arc current" (SAC) of tens to hundred of amps. The success or failure of the SPAR is contingent on the SAC being within an acceptable limit. According to the criterion in [13] if the steady-state SAC and transient recovery voltage (TRV) are within a specific zone, the SPAR (with a dead time of 500 ms) has a high probability of success. As the proposed approach considers the SAC limits, the designed transmission lines are inherently suitable for SPAR.

III. Optimized MCTLs

Optimal MCTLs can be obtained by using the methodology proposed in [9]. The methodology, modifies variables such as phase sequences, and sub-conductors' quantities, types and positions, to optimize the power capacity (surge impedance loading - SIL), costs, right of way (ROW) and height of MCTLs. Each sub-conductor is explicitly taken into account in the optimization process, with no use of the equivalent geometric mean radius (GMR) value.

Jhair S. Acosta and Maria C. Tavares are with the School of Electrical and Computer Engineering at the University of Campinas, Campinas, São Paulo, Brazil, e-mails: jhairacosta@gmail.com and ctavares@unicamp.br. Aniruddha M. Gole is a Professor of Electrical and Computer Engineering at the University of Manitoba, Winnipeg, Canada, e-mail: Aniruddha.Gole@umanitoba.ca.

We acknowledge the financial support provided by the Brazilian institutions CAPES (code 001), CNPq and FAPESP under grants 2015/26096-0, 2019/16263-7 and 2017/20010-1, and the Canadian NSERC IRC program.

Paper submitted to the International Conference on Power Systems Transients (IPST2021) in Belo Horizonte, Brazil June 6-10, 2021.

The mixed-integer non-linear mathematical model that describes the problem as a multi-objective maximization problem, inside a permutation based space, is summarized in Eqs. (1) to (6). The formulation in [9] includes a variety of electrical and mechanical constraints. However, it ignores SAC limits.

$$maximize(f_1(\vec{S}_n)+P, f_2(\vec{S}_n)+P, f_3(\vec{S}_n)+P, f_4(\vec{S}_n)+P) \tag{1}$$

with:

$$f_1(\vec{S}_n) = \frac{SIL_{(\vec{S}_n)}}{SIL_o} - 1 \tag{2}$$

$$f_2(\vec{S}_n) = 1 - \frac{Ct_{(\vec{S}_n)}}{Ct_o} \tag{3}$$

$$f_3(\vec{S}_n) = 1 - \frac{ROW_{(\vec{S}_n)}}{ROW_o} \tag{4}$$

$$f_4(\vec{S}_n) = 1 - \frac{Ht_{(\vec{S}_n)}}{Ht_o} \tag{5}$$

$$P = \sum_{c \in C} \begin{cases} \left(\frac{Cl_c - Cv_c}{Cl_c}\right) & \text{if } Cv_c > Cl_c \\ 0 & \text{otherwise} \end{cases} \tag{6}$$

where:

$\vec{S}_n$	Parameter vector which includes the tower type, circuit topology type, number of conductors in a bundle, the phase sequence, and the geometrical parameters of the circuit and bundle.
SIL_o	Sum of the surge impedance loading (SIL) of the CI conventional lines at their own voltage levels
$SIL_{(\vec{S}_n)}$	Sum of the SIL of the lines with parameter $(\vec{S}_n)$ at their own voltage levels
Ct_o	Sum of the costs of the CI conventional lines at their own voltage levels
$Ct_{(\vec{S}_n)}$	Sum of the costs of the CI lines with parameter $(\vec{S}_n)$ at their own voltage levels
ROW_o	Sum of the individual ROW of the CI conventional lines at their own voltage levels
$ROW_{(\vec{S}_n)}$	ROW for the tower with parameter $(\vec{S}_n)$
Ht_o	Sum of the individual height of the CI conventional lines at their own voltage levels
$Ht_{(\vec{S}_n)}$	Height of the tower with parameter $(\vec{S}_n)$
C	set of constraints
c	constraint
Cv_c	value of a constraint c
Cl_c	limit for the constraint c

The above multi-objective optimization problem is solved with the Non-dominated Sorting Genetic Algorithm II (NSGA-II) [14] following [9]. Nonetheless, a different multi-objective optimization algorithm could have been selected. The NSGA-II was selected because of the good performance shown in many applications [15].

However, because the above approach in [9] ignores SAC limits, there is no guarantee that the designs will permit successful SPAR, even with the use of four-legged reactor banks with large neutral reactor values [16]. In this paper, we introduce the SAC as a constraint in the mathematical model, i.e., the steady-state SAC of each circuit (SAC_{ci}) is included in the constraint-set C in (6) as in (7). This forces the SAC values to be below the limits presented in Table I, which has values extrapolated from [13].

$$SAC_{ci} \leq SAC_{ci_{limit}} \tag{7}$$

TABLE I
$SAC_{ci_{limit}}$ AND $TRV_{ci_{limit}}$ ACCORDING THE LINE VOLTAGE V_l.

V_l [kV]	138 to 345	440 to 500	750 to 1150
$SAC_{ci_{limit}}$ [A]	30	50	80
$TRV_{ci_{limit}}$ [kV]	60	100	160

Determining the steady-state SAC in each circuit could be done with Electromagnetic Transient (EMT) time-domain simulations. However, such EMT modelling would excessively slow down the optimization process. Hence, we use two-port network element to calculate the steady-sate SACs, which is is over 1000 times faster than EMT simulations. The SAC of each circuit is calculated for AG, BG and CG faults applied at 0, 50 and 100% of the line length. This is necessary because the lines are considered with a real transposition cycle of 1/6, 1/3, 1/3 and 1/6, and not as a balanced line, so the highest SAC may occur in any phase. The steady state SAC calculated by EMT and by two-port theory were found to be essentially identical. If, however, the SAC value resulting from the two-port analysis is close to or exceed the allowable SAC limit, the case is flagged for further EMT based analysis. In the EMT simulation, the case is simulated with full transient behaviour, and includes an arc model to accurately represent the arc extinction.

IV. Two-port network representation

The general representation of a two-port network is expressed in form of transmission parameters as in (8). Considering that in power systems we are interested in the current that is flowing from one node to the other, $\mathbf{I_2}$ must have a negative sign.

$$\begin{bmatrix} \mathbf{V_2} \\ -\mathbf{I_2} \end{bmatrix} = \begin{bmatrix} \mathbf{A} & \mathbf{B} \\ \mathbf{C} & \mathbf{D} \end{bmatrix} \begin{bmatrix} \mathbf{V_1} \\ \mathbf{I_1} \end{bmatrix} \tag{8}$$

A. Series impedance

The two-port network representation of a group of series impedance follows (9), where $\mathbf{Z_{s_d}}$ is the diagonal matrix comprised by the series impedance connected between $\mathbf{V_1}$ and $\mathbf{V_2}$; $\mathbf{z}$ an (n,n) zero matrix, and $\mathbf{I}$ an (n,n) identity matrix.

$$\mathbf{Q_s} = \begin{bmatrix} \mathbf{I} & -\mathbf{Z_{s_d}} \\ \mathbf{z} & \mathbf{I} \end{bmatrix} \tag{9}$$

This representation can be used for any element modeled as a series impedance, such as network equivalents and circuit-breaker status ($Z_{s_d} = 10^6$ if open, and $Z_{s_d} = 0$ if closed).

B. Transmission lines

The two-port network element for a single-phase transmission line (TL) or a positive sequence component analysis can be represented as in (10) where l is the line length, $\gamma = \sqrt{ZY}$, and $Z_c = \sqrt{ZY^{-1}}$. With Z being the series impedance and Y the shunt admittance of the line, per unit of length.

$$\begin{bmatrix} V_2 \\ -I_2 \end{bmatrix} = \begin{bmatrix} cosh(\gamma l) & -Z_c\ sinh(\gamma l) \\ \frac{-sinh(\gamma l)}{Z_c} & cosh(\gamma l) \end{bmatrix} \begin{bmatrix} V_1 \\ I_1 \end{bmatrix} \quad (10)$$

Extending the analysis to the three-phase transmission line case the **ABCD** parameters acquire dimensions of 3×3 and are represented with their modal parameters as in (11). The same form will be applied for **BCD**.

$$\mathbf{A_{mode}} = \begin{bmatrix} cosh(\gamma_{mode_1} l) & 0 & 0 \\ 0 & cosh(\gamma_{mode_2} l) & 0 \\ 0 & 0 & cosh(\gamma_{mode_3} l) \end{bmatrix} \quad (11)$$

The modal parameters can be obtained using the relationship presented in (12) to (15).

$$\mathbf{Z_{mode}} = \mathbf{T_v^{-1}} \cdot \mathbf{Z_{abc}} \cdot \mathbf{T_i} \quad (12)$$

$$\mathbf{Y_{mode}} = \mathbf{T_i^{-1}} \cdot \mathbf{Y_{abc}} \cdot \mathbf{T_v} \quad (13)$$

where:

$$\mathbf{T_v} = eigvec(\mathbf{Z_{abc}} \cdot \mathbf{Y_{abc}}) \quad (14)$$

$$\mathbf{T_i} = eigvec(\mathbf{Y_{abc}} \cdot \mathbf{Z_{abc}}) \quad (15)$$

With $\mathbf{T_v}$ and $\mathbf{T_i}$ related according (16).

$$\mathbf{T_v^{-1}} = \mathbf{T_i^{transpose}} \quad \mathbf{T_v} = inv(\mathbf{T_i^{transpose}}) \quad (16)$$

Therefore, the two-port network of a three-phase transmission line in modal domain is defined as in (17). To extend the result to the multi-circuit transmission line case the **ABCD** matrices must have dimensions of $(3n_{circ} \times 3n_{circ})$ using the corresponding modal parameters of each circuit.

$$\mathbf{Q_{TL_{mode}}} = \begin{bmatrix} \mathbf{A_{mode}} & \mathbf{B_{mode}} \\ \mathbf{C_{mode}} & \mathbf{D_{mode}} \end{bmatrix} \quad (17)$$

To be able to use the two-port network of the transmission line with the other elements of the system it is necessary to obtain its representation in phase domain ($_\phi$). To do that the following relationship between modal and phase voltages and currents for each circuit is used:

$$\mathbf{V}_\phi = \mathbf{T_v} \cdot \mathbf{V_{mode}} \quad \Rightarrow \quad \mathbf{V_{mode}} = \mathbf{T_v^{-1}} \cdot \mathbf{V}_\phi \quad (18)$$

$$\mathbf{I}_\phi = \mathbf{T_i} \cdot \mathbf{I_{mode}} \quad \Rightarrow \quad \mathbf{I_{mode}} = \mathbf{T_i^{-1}} \cdot \mathbf{I}_\phi \quad (19)$$

Leading to the phase two-port network representation in (20).

$$\mathbf{Q_{TL_\phi}} = \begin{bmatrix} \mathbf{T_v} \cdot \mathbf{A_{mode}} \cdot \mathbf{T_v^{-1}} & \mathbf{T_v} \cdot \mathbf{B_{mode}} \cdot \mathbf{T_i^{-1}} \\ \mathbf{T_i} \cdot \mathbf{C_{mode}} \cdot \mathbf{T_v^{-1}} & \mathbf{T_i} \cdot \mathbf{D_{mode}} \cdot \mathbf{T_i^{-1}} \end{bmatrix} \quad (20)$$

C. Transpositions

Long transmission lines requires transposition to reduce the voltage and line current unbalance among phases. The two-port network element of a transposition cycle can be represented in a matrix form as in (21).

$$\underbrace{\begin{bmatrix} V_{c_2} \\ V_{a_2} \\ V_{b_2} \\ -I_{c_2} \\ -I_{a_2} \\ -I_{b_2} \end{bmatrix}}_{\mathbf{VI_2}} = \underbrace{\begin{bmatrix} 0 & 0 & 1 & 0 & 0 & 0 \\ 1 & 0 & 0 & 0 & 0 & 0 \\ 0 & 1 & 0 & 0 & 0 & 0 \\ 0 & 0 & 0 & 0 & 0 & 1 \\ 0 & 0 & 0 & 1 & 0 & 0 \\ 0 & 0 & 0 & 0 & 1 & 0 \end{bmatrix}}_{\mathbf{Q_{120}}} \underbrace{\begin{bmatrix} V_{a_1} \\ V_{b_1} \\ V_{c_1} \\ I_{a_1} \\ I_{b_1} \\ I_{c_1} \end{bmatrix}}_{\mathbf{VI_1}} \quad (21)$$

Therefore, a single transposition is represented in (22), whereas as a full transposition cycle in (23).

$$\mathbf{VI_2} = \mathbf{Q_{120}} \cdot \mathbf{VI_1} \quad (22)$$

$$\mathbf{VI_2} = \mathbf{Q_{120}} \cdot \mathbf{Q_{120}} \cdot \mathbf{Q_{120}} \cdot \mathbf{VI_1} \quad (23)$$

In a generalized form for n_{circ} circuits $\mathbf{Q_{120}}$ follows the form presented in (24) with $\mathbf{rot_{120}}$ defined in (25) and $\mathbf{z}$ equal to a zero 3×3 matrix.

$$\mathbf{Q_{120}} = \begin{bmatrix} \mathbf{rot_{120}} & \mathbf{z} \\ \mathbf{z} & \mathbf{rot_{120}} \end{bmatrix} \quad (24)$$

$$\mathbf{rot_{120}} = \begin{bmatrix} 0 & 0 & 1 \\ 1 & 0 & 0 \\ 0 & 1 & 0 \end{bmatrix} \quad (25)$$

D. SLG Faults

The generalized two-port network representation for SLG faults follows (26), with $\mathbf{z}$ representing a (n, n) zero matrix, $\mathbf{I}$ an (n, n) identity matrix, and $-\mathbf{g_{fault}}$ a zero matrix with a single conductance element presented in the diagonal of the faulty phase.

$$\mathbf{Q_{fault}} \begin{bmatrix} \mathbf{I} & \mathbf{z} \\ -\mathbf{g_{fault}} & \mathbf{I} \end{bmatrix} \quad (26)$$

E. Shunt compensation

Conventionally, the SAC is mitigated by adding a four-legged reactor bank (Fig. 1) at both sides of a long transmission line In this paper, the arrangement consists of a bank of single-phase units, which is common practice for extra-high voltage levels as per IEEE Std C37.015-2017 [17]. This helps to reduce the capacitive coupling between phases that is the main cause of the SAC [11], [18] in long lines. The four-legged reactor must be designed to reduce the Ferranti effect and the SAC [11], [18]. To address the first objective, the reactor positive sequence susceptance must be equal to the line positive sequence susceptance (b_1), multiplied by a compensation factor ξ that normally varies between 0.7-0.9, and the phase reactor x_p follows (27). For SAC reduction, the capacitive coupling between phases, obtained with the zero and positive susceptance components of the line (b_0 and b_1), must be equal to the mutual susceptance of the shunt reactor. The neutral reactor x_n is then calculated as in (28) [11], [18], which is the regular approach for a balanced line.

$$x_p = 1/\xi b_1 \quad (27)$$

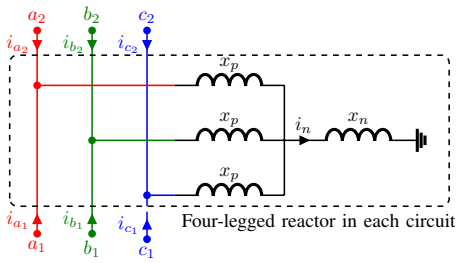

Fig. 1. Four-legged reactor scheme for two port network analysis.

$$x_n = -\frac{b_0 - b_1}{3b_1\xi(b_0 - b_1 + b_1\xi)} \tag{28}$$

From Fig. 1 the $\mathbf{A}$, $\mathbf{B}$, and $\mathbf{D}$ parameters of the two-port network representation can be easily calculated as in (29). However, $\mathbf{C}$ in (29) requires more attention.

$$\mathbf{Q_{comp}} = \left[\begin{array}{cc} \mathbf{A} = \left.\frac{\mathbf{V_2}}{\mathbf{V_1}}\right|_{\mathbf{I_1}=\mathbf{0}} = \mathbf{I} & \mathbf{B} = \left.\frac{\mathbf{V_2}}{\mathbf{I_1}}\right|_{\mathbf{V_1}=\mathbf{0}} = \mathbf{z} \\ \mathbf{C} = \left.\frac{-\mathbf{I_2}}{\mathbf{V_1}}\right|_{\mathbf{I_1}=\mathbf{0}} & \mathbf{D} = \left.\frac{-\mathbf{I_2}}{\mathbf{I_1}}\right|_{\mathbf{V_1}=\mathbf{0}} = \mathbf{I} \end{array}\right] \tag{29}$$

To obtain $\mathbf{C}$ it is necessary to write the equations that describe the system when $\mathbf{I_1} = 0$. In this situation all the current of the system will flow through the compensation reactors, yielding the equation system represented in a matrix form in (30). Therefore, $\mathbf{C}$ in (29) can be expressed as in (31).

$$\underbrace{\begin{bmatrix} V_{a_2} \\ V_{b_2} \\ V_{c_2} \end{bmatrix}}_{\mathbf{V_2}=\mathbf{V_1}} = j \underbrace{\begin{bmatrix} x_p + x_n & x_n & x_n \\ x_n & x_p + x_n & x_n \\ x_n & x_n & x_p + x_n \end{bmatrix}}_{\mathbf{X_{comp}}} \underbrace{\begin{bmatrix} I_{a_2} \\ I_{b_2} \\ I_{c_2} \end{bmatrix}}_{\mathbf{I_2}} \tag{30}$$

$$\mathbf{C} = -\mathbf{j}\mathbf{X}_{\mathbf{comp}}^{-1} \tag{31}$$

In real situations, the reactors have quality factor, so $\mathbf{jX_{comp}}$ would be replaced by $\mathbf{Z_{comp}}$. However, in the optimization process we ignored the real part of the impedance.

F. SAC calculation

To calculate the SAC, the equivalent system in Fig. 2 can be used. The fault is applied in the network section $\mathbf{Q_f}$. $\mathbf{Q_1}$ is the equivalent two-port network at left side of the fault, where as $\mathbf{Q_2}$ is the equivalent two-port network at right side of the fault.

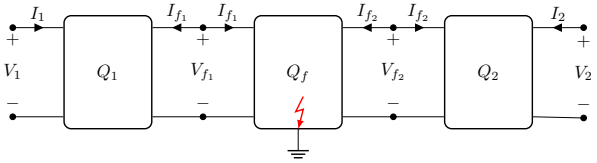

Fig. 2. Two port network equivalent of the entire system.

Eqs. (32) to (34) describe the two-port network dynamics of the system in Fig. 2.

$$\begin{aligned} \mathbf{V_2} &= \mathbf{A_2}\mathbf{V_{f_2}} + \mathbf{B_2}\mathbf{I_{f_2}} \\ -\mathbf{I_2} &= \mathbf{C_2}\mathbf{V_{f_2}} + \mathbf{D_2}\mathbf{I_{f_2}} \end{aligned} \tag{32}$$

$$\begin{aligned} \mathbf{V_{f_2}} &= \mathbf{A_f}\mathbf{V_{f_1}} + \mathbf{B_f}\mathbf{I_{f_1}} \\ -\mathbf{I_{f_2}} &= \mathbf{C_f}\mathbf{V_{f_1}} + \mathbf{D_f}\mathbf{I_{f_1}} \end{aligned} \tag{33}$$

$$\begin{aligned} \mathbf{V_{f_1}} &= \mathbf{A_1}\mathbf{V_1} + \mathbf{B_1}\mathbf{I_1} \\ -\mathbf{I_{f_1}} &= \mathbf{C_1}\mathbf{V_1} + \mathbf{D_1}\mathbf{I_1} \end{aligned} \tag{34}$$

Since $\mathbf{V_1}$ and $\mathbf{V_2}$ are known, the system given by (32) to (34) can be solved, leading to the SAC in (35).

$$\mathbf{SAC} = \mathbf{I_{f_1}} + \mathbf{I_{f_2}} \tag{35}$$

V. Tests and Results

The optimization was performed considering 10 Ω SLG faults in transmission lines of 350 km in a system like the one in Fig. 3. The four-legged reactors were calculated with (27) and (28) for a compensation level $\xi = 0.7$ in each circuit. The sources were adjusted to transmit 90% of the line SIL. The sending equivalent has a short circuit ratio (SCR) = 25, and the receiving equivalent a SCR = 15. In all cases, SCR = 1 is the current when transmitting 100% of the line SIL.

The secondary arc does not present the same response for all networks, but rather is influenced by the specific network seen at line terminals. In the present research, equivalent systems described above were considered at both line terminals to demonstrate the basic concept. In an actual utility-level study, the system equivalents should include eventual transformer arrangements with specific grounding systems.

A. Optimal MCTLs

Consider the case of the optimized MCTL in Fig. 4 with a double circuit transmission line operating at 500 kV. The design has been optimized using (1) to (6) and the additional SAC constraint (7). The NSGA-II optimization had a population of 100 individuals evolving during 1000 generations. As can be observed, the optimized line presents maximum RMS SAC values of 47 A and 49 A in circuit one and two, respectively, which are lower than the limits in Table I.

Without the SAC constraint (7) the line design is as in Fig. 5, which is quite different from the line configuration obtained with the SAC constraint in Fig. 4. It is clear that this is a direct result of the SAC inclusion in the optimization process, considering that both lines were designed with four-legged shunt reactor bank calculated with the Kimbark formulation.

The maximum SAC for the line in Fig. 5 is ≈ 109 A, which violates the SAC constraint in Table I. Thus a line designed by ignoring the SAC constraint would not guarantee a successful SPAR. However, the SAC reduction has an associated cost. By comparing Fig. 4 (optimized with SAC constraint) and Fig. 5 (without SAC constraint), it is evident that SAC reduction was made possible only with a larger conductor height and a lower power capacity (SIL). Also, note that the line in Fig. 4 has a y_0 approximately 24% smaller than the line in Fig. 5.

All previous HSIL lines proposed in different researches had regular zero sequence admittance values, and, as far as the authors are aware of, for the first time the proposed optimization model is modifying this feature. Thus, this characteristic is contributing to the SAC reduction from the tower design (its origin), and not only by using mitigation resources as four-legged reactors.

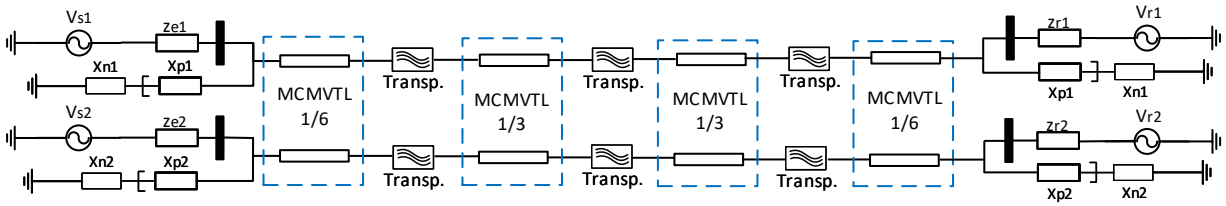

Fig. 3. Test system representation.

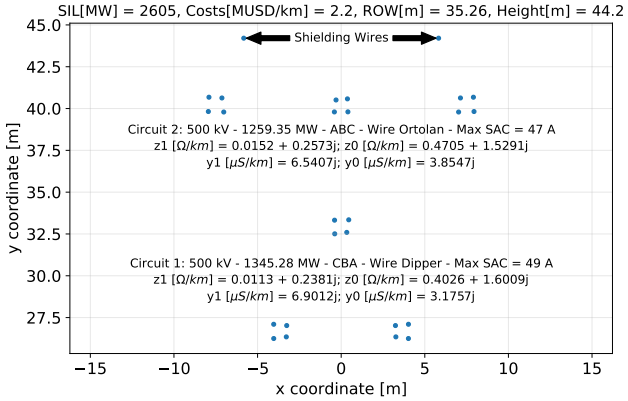

Fig. 4. Optimal MCTL including SAC optimization.

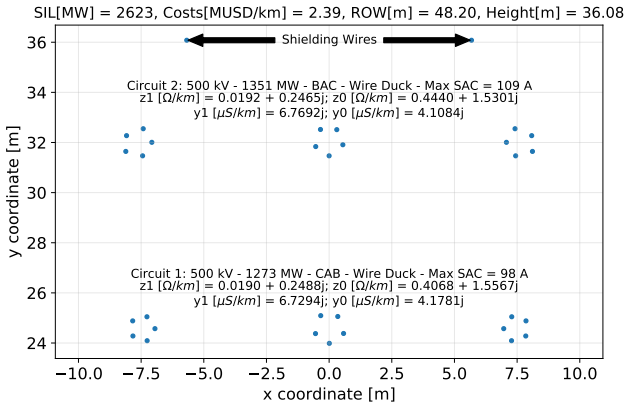

Fig. 5. Optimal MCTL without including SAC optimization.

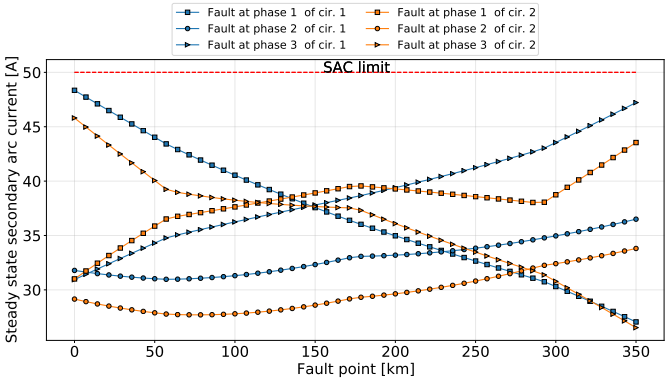

Fig. 6. SAC along the optimized MCTL with SAC restriction.

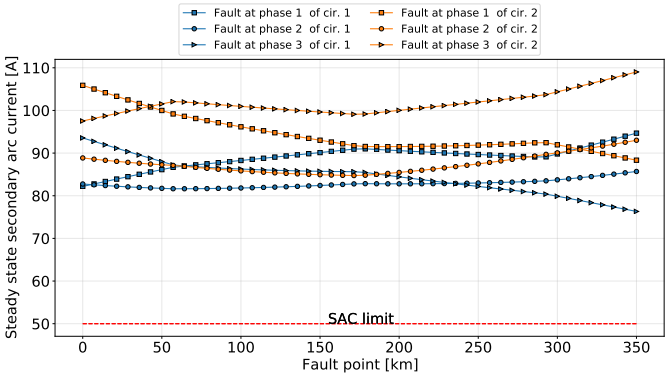

Fig. 7. SAC along the optimized MCTL without SAC restriction.

The RMS steady state SAC as a function of the fault position along the lines in Fig. 4 and 5 is presented in Fig. 6 and 7, respectively. As expected, the SAC values are larger at line terminals. In the case of the TL with SAC restriction, the larger SAC value occurred for a fault close to the sending end (high SCR). However, in the line without SAC restriction the larger SAC value was produced by a fault in the receiving end (low SCR). Also, note that depending on the faulted phase, the larger SAC value will be either at the sending end, or at the receiving end. Hence, it is evident that during the optimization process it is necessary to consider the SAC for faults in each phase and at both line ends, once the actual transposition cycles are considered.

The RMS transient recovery voltage (TRV) for faults along the previous lines is presented in Figs. 8 and 9. It is possible to observe that as in the case of the SAC behavior, the MCTL designed with the SAC restriction presents TRV values under the maximum limits. Therefore, there is a high probability of a successful SPAR. On the other hand, the MCTL designed without the SAC restriction presents TRV values above the limit. Hence, it is clear that including the SAC in the optimization model not only helps in the SAC mitigation, but also in the TRV reduction.

B. Optimal Multi-Circuit Multi Voltage Transmission Lines (MCMVTLs)

Multi-circuit configurations with different voltage levels on each circuit can also be optimized using the proposed methodology. A double-circuit transmission line with circuit 1 at 500 kV and circuit 2 at 750 kV was optimized. Fig. 10 shows the optimized line when considering the SAC as a

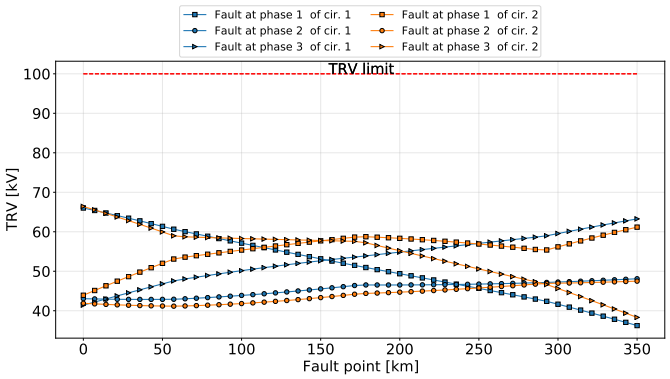

Fig. 8. RMS TRV along the optimized MCTL with SAC restriction.

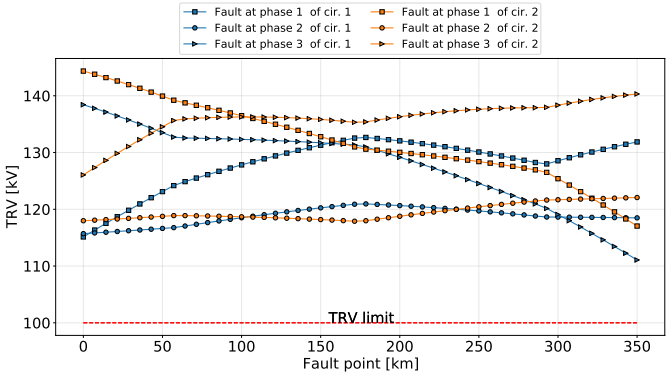

Fig. 9. RMS TRV along the optimized MCTL without SAC restriction.

restriction. Meanwhile, Fig. 11 shows the optimized line when the SAC is not considered as a restriction.

Using a similar test case as the MCTL case, the MCMVTLs were also connected to an ac system with short circuit ratio (SCR) = 25 at the sending end a system of SCR = 15 at the receiving end [10], considering a loading of 90% of the line SIL at each circuit.

Fig. 12 shows SAC as a function of the fault position and faulted phase with the SAC constraint. It can be seen that SAC for both circuits is below the permissible limits of 50 A for circuit 1 and 80 A for circuit 2. On the other hand, without the SAC constraint as seen in Fig. 13 the maximum SAC in circuit 1 exceeds the SAC limit for circuit 1.

Thus it is evident that ignoring the SAC constraint results in an unacceptably large SAC of 115 A on circuit 1 (note that the SAC limit is 50 A). On the other hand, using the SAC constraint yields an acceptable SAC of 45 A.

However, there is also an associated cost caused by including the SAC constraint. The SAC reduction was achieved with an increased line cost, ROW and tower height.

Note that in this case a reduction of approximately 13% of the zero sequence admittance y_0 of the first circuit was also achieved, helping with the SAC mitigation. Also, as was the case of the MC lines, the TRV behavior is similar to the SAC behavior, so it is not shown here.

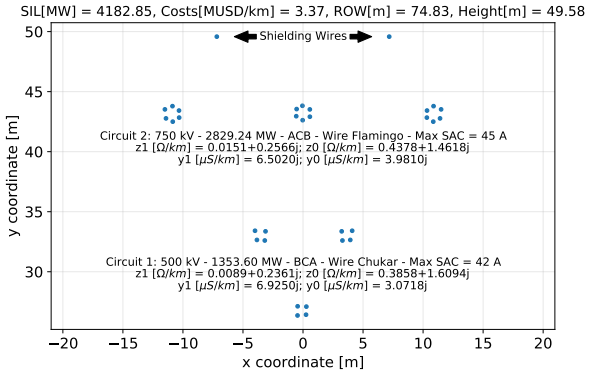

Fig. 10. Optimal MCMVTL including SAC optimization.

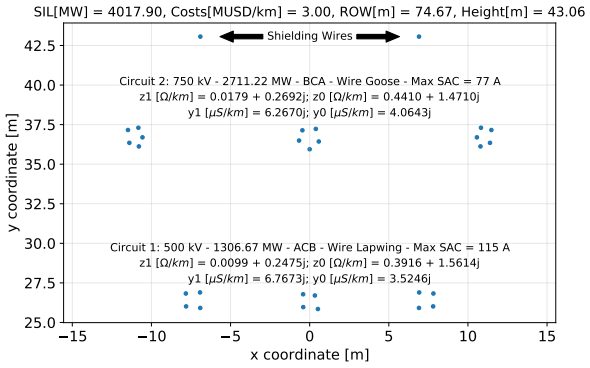

Fig. 11. Optimal MCMVTL without including SAC optimization.

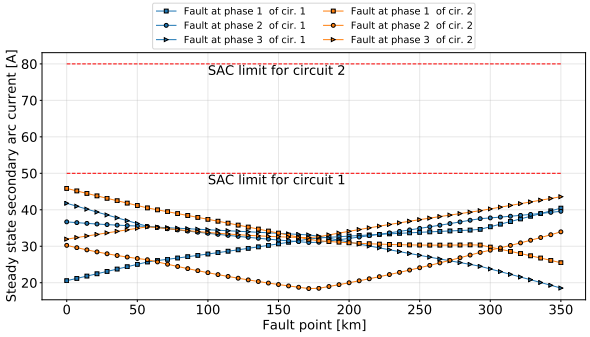

Fig. 12. Secondary arc current along the optimized MCMVTLs with SAC restriction.

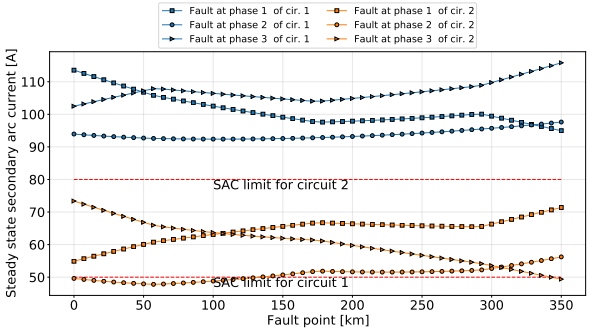

Fig. 13. Secondary arc current along the optimized MCMVTLs without SAC restriction.

C. Neutral reactor comparison

Table II shows a comparison between the neutral reactor of the lines in Figs. 4, 5, 10, and 11. It is clear that although the phase reactors x_{p_1} and x_{p_2} are relatively close in value, their neutral reactors x_{n_1} and x_{n_2} are considerably different. The former is expected, because there are no important changes in the SIL of those lines, meanwhile, the zero sequence admittance has been drastically reduced in the cases where the SAC reduction was high.

When the SAC constraint is ignored, much smaller neutral reactors (under 750 Ω) are obtained, whereas considering the SAC constraint results in larger neutral reactor for both circuits. It is interesting to observe that the highest values were presented in the circuit one (more than 1100 Ω), which is not an expected result. This is caused by the configuration of the circuits in the transmission lines. Thus, the optimized transmission lines with the SAC restrictions presented a more compact configuration for the first circuit, yielding to higher neutral reactors. Therefore, other TL configurations with both circuits being compact would lead to similar neutral reactor values in both circuits.

TABLE II
NEUTRAL REACTOR COMPARISON BETWEEN THE LINE WITH AND WITHOUT SAC OPTIMIZATION.

Line Type	$x_{p_1}[\Omega]$	$x_{p_2}[\Omega]$	$x_{n_1}[\Omega]$	$x_{n_2}[\Omega]$	$V_{n_1}[kV]$	$V_{n_2}[kV]$
Fig. 4	1162.97j	1226.56j	1142.86j	495.77j	61	46
Fig. 5	1211.81j	1132.71j	526.34j	368.21j	47	42
Fig. 10	1159.08j	1234.05j	1309.77j	435.75j	64	64
Fig. 11	1185.58j	1280.07j	745.40j	361.60j	55	58

Table II shows an additional trade-off when optimizing the lines considering the SAC restriction: the neutral reactor value is larger, but there is a marginal increase in the neutral reactor voltages $V_{n_{ci}}$.

D. Detailed Arc Model

To finalize the feasibility study of the SPAR, the detailed A. T. Johns arc model described by (36) to (38) [19] was used on the EMT program PSCAD. Both, the stationary arc conductance G and the arc conductance g are in [S].

$$\frac{\delta g_k}{\delta t_k} = \frac{1}{\tau_k(t_k)}\left[G_k(t_k) - g_k(t_k)\right] \tag{36}$$

$$G_k(t) = \frac{|i_k(t)|}{V_k l_k(t)} \tag{37}$$

The model is applicable for both the primary and the secondary arc. The sub-index k equals p for the primary arc and s for the secondary arc. Hence, i_k is the instantaneous arc current, t_k the time from the initiation of the arc, $V_p = 15$ V/cm, $l_p(t)$ is equal to 1.1 times the insulator string length (l_0), $V_s = 75 I_s^{-0.4}$ V/cm, I_s is the steady state peak SAC in [A], and $l_s(t_s)$ is equal to $1.1 l_0$ for $t_s < 0.1s$ and $1.1 l_0 t_s$ for $t_s \geq 0.1s$.

The time constant τ_k, is calculated as in (38), where I_p and I_s are the steady state peak primary and secondary arc currents in [A].

$$\tau_p(t_p) = \frac{2.85\ 10^{-5} I_p}{l_p(t_p)} \quad \tau_s(t_s) = \frac{2.51\ 10^{-3} I_s^{1.4}}{l_s(t_s)} \tag{38}$$

The arc extinction criterion in [19] is based on the electrostatic re-ignition verified at each SAC zero crossing. If the absolute value of the open circuit arc voltage is lower than the absolute value of the arc withstand voltage $|v_w|$ in [kV], calculated as in (39), the arc is finally extinguished.

$$|v_w(t_s)| = \left[5 + \frac{1620 T_e}{2.15 + I_s}\right](t_s - T_e) l_s(t_s) h(t_s - T_e) \tag{39}$$

The extinction time T_e is a discrete value that is updated each time that the arc current has a zero crossing. Meanwhile, $h(t_s - T_e)$ is a delayed step function that is 0 for $t_s < T_e$ and 1 for $t_s > T_e$ [19].

The simulations with the arc model were performed in PSCAD with a component that gets as input l_0, I_p and I_s. It was considered $l_0 = 400$ cm for 500 kV lines, and $l_0 = 646$ cm for 750 kV lines. Meanwhile, the I_p and I_s values were previously calculated with two-port networks elements for all the fault points.

Table III shows the maximum arc extinction times values obtained in different lines. As can be seen, it is confirmed that the optimization yield lines for which the arc extinction time is much smaller, almost 50% of that for lines optimized without the SAC constraint. This agrees with the RMS SAC reduction. However, the extinction times in practical situations will vary according to stochastic environmental variables such as wind speed, environmental temperature etc. Hence, the values in Table III are not definitive, but shows that the RMS SAC reduction indeed yield smaller arc extinction times.

TABLE III
MAXIMUM SAC EXTINCTION TIME IN $[ms]$ FOR DIFFERENT LINES.

Line Type	$t_{ext_{ci_1}}$	$t_{ext_{ci_2}}$
Fig. 4	285.66	295.98
Fig. 5	485.49	485.18
Fig. 10	247.11	262.75
Fig. 11	529.75	376.28

Figs. 14 and 15 show the worst arc current and voltage waveform obtained in the MCTL of Fig. 4 for a SLG fault. Fig. 16 shows the worst SAC in the line of Fig. 5. We can clearly see that the line in Fig. 4 presents lower SAC, TRV and arc extinction time than the line in Fig. 5. Therefore, the advantages of including the SAC in the optimization model are clearly evidenced. The response of the lines in Figs. 10 and Fig. 11 is similar, so they are not presented here.

VI. CONCLUSIONS

Single-phase auto reclosing in transmission lines is a key feature which enables some power transmission even during single line to ground faults. A successful SPAR demands that the secondary arc current and transient recovery voltage do not exceed certain limits. In single circuit long lines this can be easily achieved by using four-legged reactors following the formulation proposed by Kimbark [11]. However, in multi-circuit transmission lines it is not straightforward and special neutral reactor configurations must be considered [16]. This is a result of additional inter-circuit capacitive coupling that must be compensated by higher neutral reactor values.

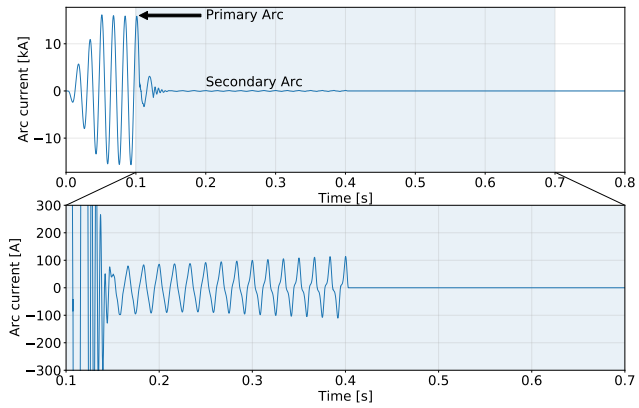

Fig. 14. Worst arc current (top) and secondary arc current (zoomed, bottom) for a SLG fault in the line of Fig. 4 using the Johns model [19].

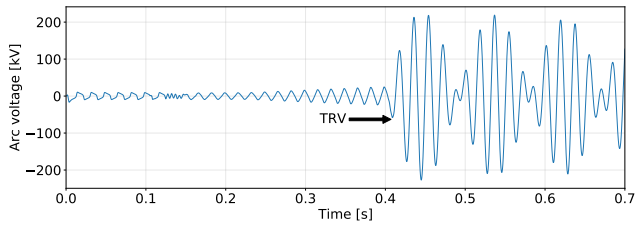

Fig. 15. Arc voltage for the worst SAC for a SLG fault in the line of Fig. 4 using the Johns model [19].

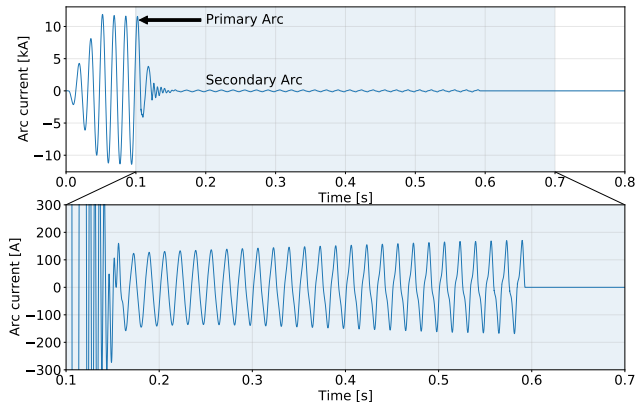

Fig. 16. Worst arc current (top) and secondary arc current (zoomed, bottom) for a SLG fault in the line of Fig.5 using the Johns model [19].

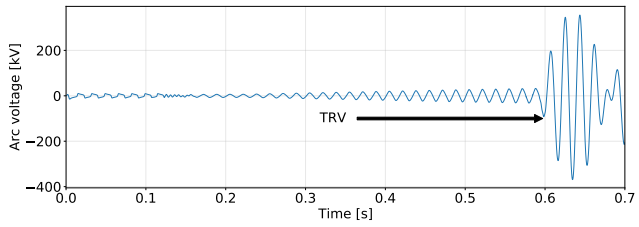

Fig. 17. Arc voltage for the worst SAC for a SLG fault in the line of Fig. 5 using the Johns model [19].

This paper proposes an innovative solution to this problem by including the SAC as a constraint in the optimization procedure during the design of the transmission lines. Thus, the maximum SAC reduction achieved in the test cases was almost 64%, compared with the cases that do not consider the SAC during the optimization process. Finally, since the lines obtained with the proposed model have SAC values under the limits, the HSIL transmission lines obtained with this approach are adequate for SPAR.

REFERENCES

[1] G. N. Alexandrov and G. V. Podporkyn, "Improvement of the efficiency of 35 to 220 kV lines," *Int. Conf. AC DC Power Transm.*, no. 5, pp. 226–231, 1991.

[2] J. C. Salari, "Optimizing Transmission Lines Conductors Bundle Geometries (in Portuguese)," Master Thesis, Federal University of Rio de Janeiro, Brazil, 1993.

[3] S. Gomes Jr, C. Portela, and C. Fernandes, "Principle and advantages regarding the use of lnpe's and presentation of comparative results (in portuguese)," in *XIII Semin. Nac. Produção e Transm. Energ. Elétrica*, Florianópolis, SC, Brazil, 1995.

[4] C. Portela and S. Gomes, "Analysis and optimization of non conventional transmission trunks, considering new technological possibilities," in *Proc. VI SEPOPE*, vol. SP-092, no. 1, Salvador, BA, Brazil, 1998, pp. 1–6.

[5] J. S. Acosta and M. C. Tavares, "Transient Behavior of High Surge Impedance Loading Transmission Lines," in *Int. Symp. High Volt. Eng.*, vol. 2, no. 3, Buenos Aires, Argentina, 2017.

[6] ——, "Methodology for optimizing the capacity and costs of overhead transmission lines by modifying their bundle geometry," *Electr. Power Syst. Res.*, oct 2017.

[7] M. F. Ribeiro, J. A. Vasconcelos, and D. A. Teixeira, "Optimization of compact overhead lines of 138/230kV: Optimal selection and arrangement of cables and definition of the best transmission line tower topology," in *17th IEEE Int. Conf. Environ. Electr. Eng. 1st IEEE Ind. Commer. Power Syst. Eur. EEEIC / I CPS Eur.*, 2017.

[8] J. S. Acosta and M. C. Tavares, "Optimal selection and positioning of conductors in multi-circuit overhead transmission lines using evolutionary computing," *Electric Power Systems Research*, vol. 180, p. 106174, 2020.

[9] ——, "Multi-objective optimization of overhead transmission lines including the phase sequence optimization," *International Journal of Electrical Power & Energy Systems*, vol. (115), p. 105495, 2020.

[10] ——, "Transient behaviour of non-conventional multi-circuit power lines with different voltages levels at the same tower," in *Int. Conf. Power Syst. Transients*, Perpignan, France, 2019, p. 6.

[11] E. W. Kimbark, "Suppression of Ground-Fault Arcs on Single-Pole-Switched EHV Lines by Shunt Reactors," *IEEE Transactions on Power Apparatus and Systems*, vol. 83, no. 3, pp. 285–290, 1964.

[12] IEEE, "IEEE Guide for Automatic Reclosing of Circuit Breakers for AC Distribution and Transmission Lines," pp. 1–72, 2012.

[13] A. Balossi, M. Malaguti, and P. Ostano, "Laboratory full-scale tests for determination of the secondary arc extinction time in high-speed reclosing," in *IEEE Summer Power Meet. July 10-15*, New Orleans, 1966.

[14] K. Deb, A. Pratap, S. Agarwal, and T. Meyarivan, "A fast and elitist multiobjective genetic algorithm: NSGA-II," *IEEE Trans. Evol. Comput.*, vol. 6, no. 2, pp. 182–197, 2002.

[15] J. Del Ser, E. Osaba, D. Molina, X.-S. Yang, S. Salcedo-Sanz, D. Camacho, S. Das, P. N. Suganthan, C. A. Coello Coello, and F. Herrera, "Bio-inspired computation: Where we stand and what's next," *Swarm and Evolutionary Computation*, vol. 48, pp. 220 – 250, 2019.

[16] J. S. Acosta Sarmiento, M. C. Tavares, and A. M. Gole, "Neutral reactor structures for improved single phase auto reclosing in non-conventional multi-circuit multi-voltage transmission lines," *IEEE Transactions on Power Delivery*, pp. 1–1, (Early Access) 2021.

[17] IEEE, "Ieee guide for the application of shunt reactor switching," *IEEE Std C37.015-2017 (Revision of IEEE Std C37.015-2009*, pp. 1–63, 2018.

[18] N. Knudsen, "Single Phase Switching of Transmission Lines Using Reactors For Extinction of The Secondary Arc," in *Conférence Internationale des Grands Réseaux Électriques à Haute Tension*, vol. 33, Paris - France, 1962, pp. 1–7.

[19] A. Johns, "Improved techniques for modelling fault arcs an faulted EHV transmission systems," *IEE Proc. - Gener. Transm. Distrib.*, vol. 141, no. 2, p. 148, 1994.